Green synthesis and characterisation of $ZnMn_2O_4$ nanoparticles for photocatalytic degradation of Congo red dye and kinetic study

Saeid Taghavi Fardood[1], *Farzaneh Moradnia*[1], *Ali Ramazani*[1,2] ✉

[1]*Department of Chemistry, University of Zanjan, P O Box 45195-313, Zanjan, Iran*
[2]*Research Institute of Modern Biological Techniques (RIMBT), University of Zanjan, P O Box 45195-313, Zanjan, Iran*
✉ *E-mail: aliramazani@gmail.com*

Published in Micro & Nano Letters; Received on 28th January 2019; Revised on 3rd April 2019; Accepted on 25th April 2019

In this work, $ZnMn_2O_4$ spinel nanoparticles were successfully synthesised by tragacanth gel through the easy and inexpensive novel sol–gel method. This technique has many strong points such as facile, economical, non-toxic and quickness in comparison with other methods. The zinc manganite nanoparticles were characterised by X-ray powder diffraction (XRD), transmission electron microscopy, field emission scanning electron microscopy, Fourier transform infrared spectroscopy and diffuse reflectance spectroscopy. The XRD pattern confirmed the formation of spinel tetragonal structure of $ZnMn_2O_4$ nanoparticles with a crystallite size of 14 nm. The degradation of Congo red dye by synthesised nanoparticles was studied using employing UV–Vis spectroscopy. The $ZnMn_2O_4$ NPs expressed high photocatalytic activity for degradation of Congo red dye at room temperature in aqueous solution so that 96% of Congo red was degraded in 15 min. The spinel $ZnMn_2O_4$ photocatalyst provided total organic carbon removal as 45.2% in 15 min. The spinel $ZnMn_2O_4$ NPs reusability was examined by administering the degradation of Congo red dye with the spent catalyst and it was considered that the photocatalyst did not exhibit any significant reduction in its activity even after three cycles.

1. Introduction: Approximately 15% of the total world manufacture of dyes is lost during the dyeing process and is released in the textile sewerages [1, 2]. The release of those coloured wastewaters in the ecosystem is a demonstrative source of non-aesthetic pollution, eutrophication and perturbations in the aquatic life. As international environmental standards are becoming more stringent (ISO 14001, October 1996), technological systems for the removal of organic pollutants, such as dyes have been recently expanded. Between them, physical methods, such as biological methods (biodegradation) [3, 4], adsorption [5, 6] and chemical methods (chlorination, ozonation [7]) are the most frequently used. Photocatalysis is considered as one of the important and efficient approaches to dismiss the dyes in wastewater [8–16]. Different methods have been provided for the synthesis of nanoparticles such as chemical, physical and green methods [17, 18]. Lately, researchers focus on green chemistry methods to provide metal nanoparticles with favourable size and morphology and the results of this method are significant and important [19–22]. In the last decade, preparing the nanocatalyst via photocatalytic capability by using green synthesis methods has been an idea for researchers. Plant extracts for the biological synthesis of nanoparticles have received more attention because it is inexpensive, simple, environmentally safe and non-toxic [23–26]. Further, most of the plant extracts are fortified by the variety of biomolecules like alkaloids, phenols, terpenoids, flavonoids and so on [27–35]. In this work, we report the synthesis of spinel $ZnMn_2O_4$ NPs via novel biological way and use the tragacanth gel to provide sol–gel. We have studied the photocatalytic activity of $ZnMn_2O_4$ using followed degradation of Congo red as the industrial dye in aqueous solution under visible irradiation. X-ray powder diffraction (XRD), Fourier transform infrared spectroscopy (FTIR), transmission electron microscopy (TEM), diffuse reflectance spectroscopy (DRS) and field emission scanning electron microscopy (FESEM) are the techniques that we used for the characterisation of biosynthesised $ZnMn_2O_4$. The chemical structure of Congo red is shown in Fig. 1.

2. Experimental
2.1. General information: The tragacanth gum (TG) was prepared from a native health food store. The $Zn(NO_3)_2.6H_2O$ and $Mn(NO_3)_2.4H_2O$ were purchased from Merck. Congo red was purchased from Merck and had used without further refinement. The structural properties of $ZnMn_2O_4$ NPs were confirmed by XRD technique on X'Pert-PRO advanced diffractometer using Cu (Kα) radiation (wavelength: 1.5406 Å), operated at 40 kV and 40 mA at room temperature in the range of 2θ from 10 to 80. The external structure of this sample was determined by a Jasco 6300 FTIR spectroscopy. The FTIR spectrum was collected between the wave number of 400 and 4000 cm^{-1}. Measurements were accomplished with KBr technique. UV–Vis absorption spectra were prepared on a Metrohm (Analytical Jena-Specord 205) double-beam instrument. The diffuse reflectance UV–Vis spectroscopy of the as-prepared sample was recorded by a UV–Vis spectrophotometer (Shimadzu, UV-2550, Japan) by using $BaSO_4$ as a reference. The compound morphology and size of the sample surfaces were studied by scanning electron microscope (Zeiss EVO 18, Germany). The TEM analysis of the catalyst was conducted using a Philips CM30. The degradation of Congo red was followed by using total organic carbon (TOC) analyser (Shimadzu TOC-5000).

2.2. Synthesis of spinel $ZnMn_2O_4$ NPs: $Zn(NO_3)_2.6H_2O$ and $Mn(NO_3)_2.4H_2O$ were used as starting materials for the synthesis of $ZnMn_2O_4$ NPs. In the first step, 0.2 g of the TG was blended and dissolved in 40 ml of deionised water and stirred for 80 min at 70°C. In the next step, 2 mmol of $Mn(NO_3)_2.4H_2O$ and 1 mmol of $Zn(NO_3)_2.6H_2O$ were added to the TG solution. After that, the container containing the gel was moved to a sand bath. The sand bath temperature was stabled at 75°C and stirring was consecutive for 12 h. The product of this step was the brown colour resin. In the next step, this resin was calcined in air at 600°C for 4 h to obtain spinel $ZnMn_2O_4$ NPs.

2.3. Photocatalytic reactor: Experiments were carried out in a batch mode photoreactor. The irradiation origin was a fluorescent lamp ($\lambda >$ 400 nm, 90 W, Parmis, Iran), which was put above the batch photoreactor. The reaction was manufactured in conditions: Congo red = 20 mg/l, catalyst = 0.03 g, pH = natural and room temperature.

Micro & Nano Letters, 2019, Vol. 14, Iss. 9, pp. 986–991
doi: 10.1049/mnl.2019.0071

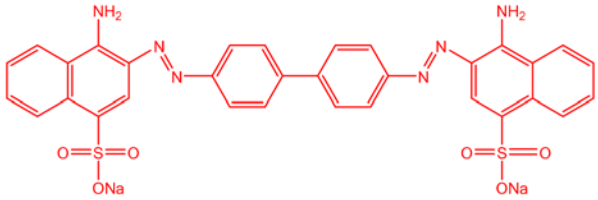

Fig. 1 *Structure of Congo red dye*

2.4. Photocatalytic dye degradation: Congo red was selected to check the photocatalytic dye degradation of $ZnMn_2O_4$ NPs. This experiment was investigated under the visible light. Degradation of Congo red was followed in the presence and absence of visible light in aqueous solution. Hereon, 50 ml solution of dye with 20 mg/l concentration was ready and 0.03 g of NPs sample was dispersed in it. The solutes above nanophotocatalyst were taken out from the reaction environment at regular time cycles. The centrifuge was used for separating the $ZnMn_2O_4$ NPs from solution and the absorbance alteration was followed at a maximum wavelength (λ_{max}) of dye (496 nm) by UV–Vis spectrophotometer (Analytical Jena-Specord 205). Following equation was used for the calculation of degradation percentages:

$$\%\text{Degradation} = (A_0 - A_t)/A_0 \times 100$$

3. Results and discussion

3.1. Characterisation of $ZnMn_2O_4$ nanoparticles: FTIR spectra were registered in solid phase using the KBr pellet technique in the range of 400–4000 cm^{-1}. This technique was exploited to stabilise the formation of metal–metal (M–M) bonds and metal–oxygen (M–O) in the spinel structure of the sample. Fig. 2 display FTIR absorption spectra of $ZnMn_2O_4$ NPs calcined at 600°C for 4 h. The FTIR spectrum analysis demonstrates two ranges of the absorption bands: in the range of 400–1000 cm^{-1}, two absorption bands for the spinel structure of the $ZnMn_2O_4$ ν_1 at 621 cm^{-1} and ν_2 at 507 cm^{-1} were observed. The band, ν_1, suggests the stretching vibrations of the metal (Mn ↔ O) and the ν_2 is attributed to stretching vibrations of the metal (Zn ↔ O) [36]. These are the first evidence of $ZnMn_2O_4$ formation.

The phase and structural determination of the spinel $ZnMn_2O_4$ nanoparticles was confirmed by XRD technique. The XRD pattern of the $ZnMn_2O_4$ nanoparticles is shown in Fig. 3. As shown in Fig. 3, the diffraction peaks at 2θ of 18.31°, 29.45°, 31.27°, 33.02°, 36.44°, 38.96°, 44.81°, 50.90°, 52.12°, 54.66°, 56.85°, 59.08°, 60.88°, 65.36°, 71.17°, 75.15° and 77.57° are corresponded to (101), (112), (200), (103), (211), (004), (220), (204), (105), (312), (303), (321), (224), (400), (305), (413) and (422) planes of the tetragonal spinel $ZnMn_2O_4$ NPs, respectively. All the diffraction peaks were readily indexed to a pure phase tetragonal spinel structure (JCPDS Card No. 77-0470).

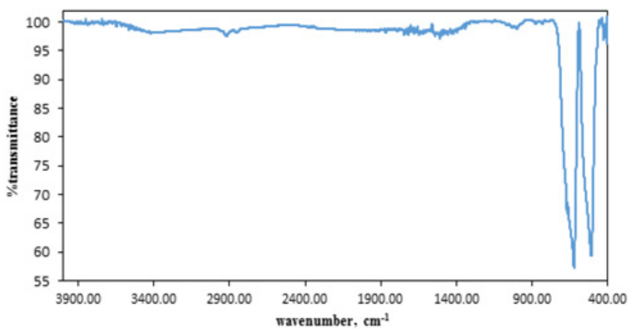

Fig. 2 *FTIR spectrum of $ZnMn_2O_4$ NPs*

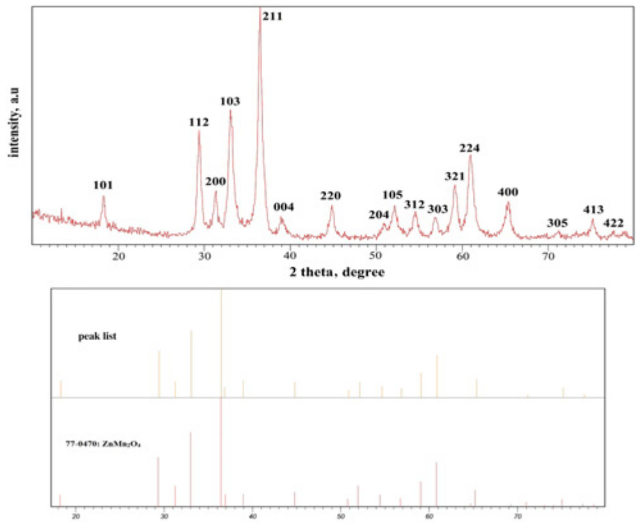

Fig. 3 *XRD pattern of $ZnMn_2O_4$ NPs*

No diffraction peaks of other impurities were detected. The average crystallite size of $ZnMn_2O_4$ nanoparticles was distinguished from the full width at half maximum (FWHM) of the (211) diffraction peak using the Scherrer formula:

$$D = 0.9\lambda/\beta\cos\theta$$

where D is the crystallite size (nm), β is the FWHM of the peak, λ is the X-ray wavelength of Cu Kα = 0.154 nm and θ is the Bragg angle [26]. Using the above equation, we gained an average crystallite size of 14 nm for $ZnMn_2O_4$ NPs.

Fig. 4 shows the FESEM image of green synthesised $ZnMn_2O_4$ NPs that calcined at 600°C for 4 h. It can be seen from the FESEM image that the $ZnMn_2O_4$ NPs have narrow size distributions and fairly uniform spherical shape.

Acceptable results from FESEM and XRD technique are confirmed by the TEM image (Fig. 5). This image shows the morphology and particle size of the $ZnMn_2O_4$ NPs. the $ZnMn_2O_4$ NPs morphology is spherical with a regular particle size of about 30–45 nm.

Measurement of optical absorption feature and electronic state of $ZnMn_2O_4$ nanoparticles were surveyed by DRS. The bandgap

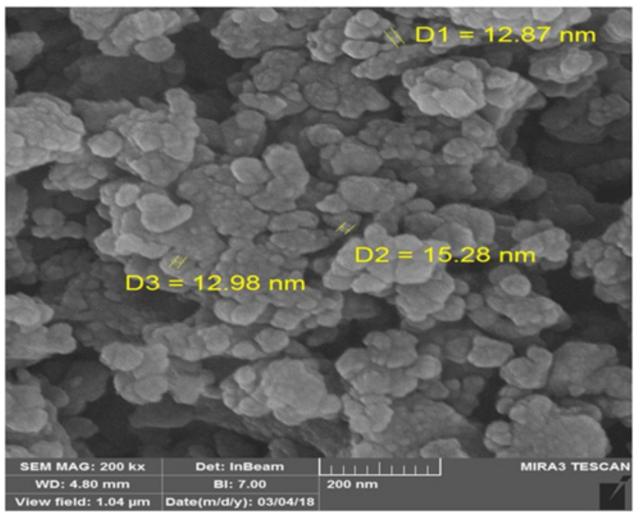

Fig. 4 *SEM micrograph of the $ZnMn_2O_4$ NPs*

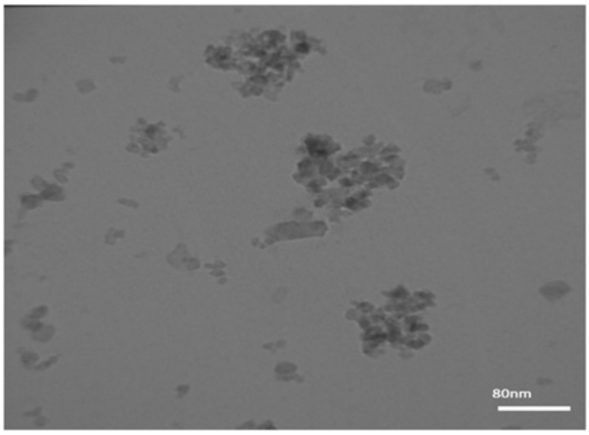

Fig. 5 *TEM micrograph of the $ZnMn_2O_4$ NPs*

energy was measured using a reflectance technique by exerting the Tauc theory (1) [37]

$$(\alpha h\nu)^2 = A(h\nu - E_g) \quad (1)$$

α, $h\nu$, A and E_g are the absorption coefficients, the energy of the incident photon, edge width parameters independent of photon energy and the bandgap of the material, respectively. The bandgap of the nanoparticle was acquired using Tauc's graph of $(\alpha h\nu)^2$ against $h\nu$ (Fig. 6), extrapolating the linear section of the absorption edge to find the intercept by energy axis. The consequence showed that the bandgap of $ZnMn_2O_4$ is about 1.82 eV. Therefore, it is confirmed that $ZnMn_2O_4$ NPs is the efficient photocatalyst in a visible-light region.

The synthesised $ZnMn_2O_4$ NPs were considered as a photocatalyst for degradation of the Congo red dye in the presence of visible light irradiation and air at room temperature.

3.2. Effect of visible light irradiation and $ZnMn_2O_4$ NPs catalyst: In this work, the photocatalytic activity of $ZnMn_2O_4$ on degradation of Congo Red dye was measured under three conditions: nanophotocatalyst under visible light irradiation, nanophotocatalyst under dark and visible light irradiation without $ZnMn_2O_4$. In the state without a catalyst, we do not have any degradation. So long as using $ZnMn_2O_4$ catalyst under dark condition, we see the removal of 41%. Fig. 7 shows when light and catalyst are applied at the same time, 96% of Congo red dye was degraded at 15 min.

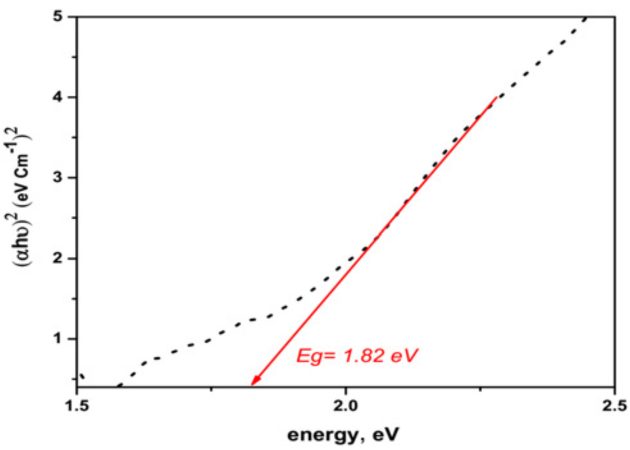

Fig. 6 *Tauc plot of the $ZnMn_2O_4$ NPs*

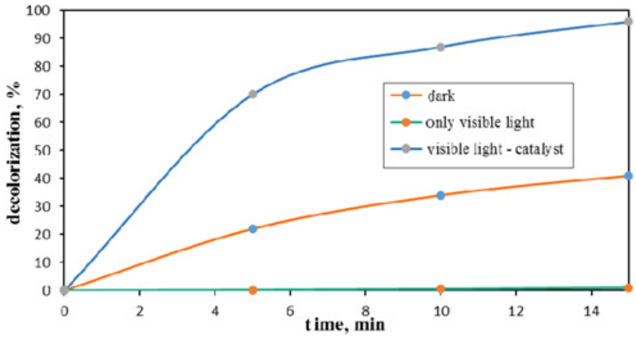

Fig. 7 *Effect of visible light irradiation on the decolourisation efficiency (%). Reaction conditions: Congo red = 20 mg/l, catalyst = 0.03 g, pH = natural and room temperature*

3.3. Effect of photocatalyst dosage: For considering the effect of photocatalyst dosage on decolourisation, various amounts of the $ZnMn_2O_4$ NPs was examined. In this test, 0.01–0.04 g of catalyst was used in 20 mg/l concentration of Congo red dye and at a fixed time of 15 min. Fig. 8 demonstrates the photocatalyst effect of $ZnMn_2O_4$ on decolourisation of dyes percentages for 15 min. It can be considered that increasing the catalyst concentration causes the increase of removal of dye.

3.4. Effect of initial dye concentration: Photocatalytic degradation of Congo red dye by $ZnMn_2O_4$ nanocatalyst under visible irradiation was followed by modifying the incipient Congo red concentration (10, 20, 30 and 40 mg/l) in presence of constant $ZnMn_2O_4$ dosage (0.03 g). The process of variation photocatalytic degradation yield by changing the initial Congo red concentration is illustrated in Fig. 9. It can be realised that the photocatalytic

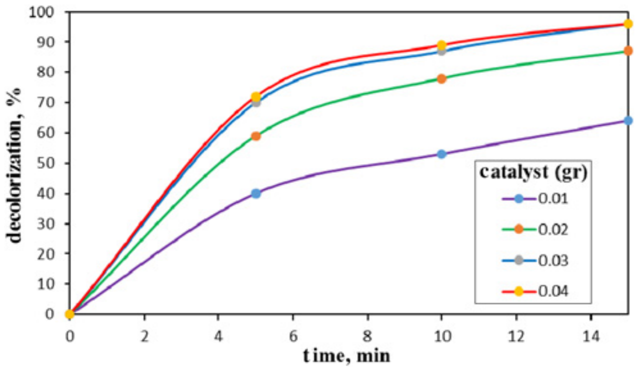

Fig. 8 *Effect of photocatalyst dosage on the photocatalytic degradation of Congo red dye (pH = natural, Congo red = 20 mg/l)*

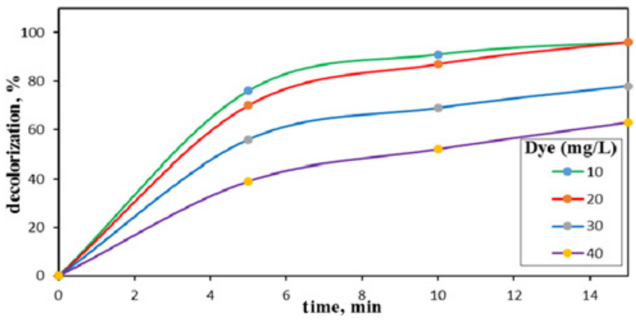

Fig. 9 *Effect of initial concentration of Congo red dye on the decolourisation efficiency (%)*

doi: 10.1049/mnl.2019.0071

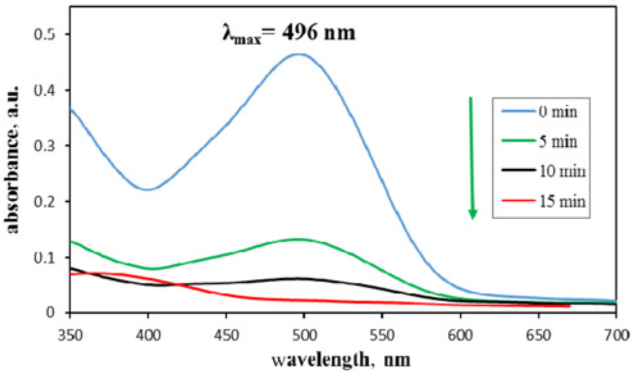

Fig. 10 *Absorption spectra of Congo red solutions (20 mg/l) in the presence of 0.03 g of $ZnMn_2O_4$ photocatalyst under visible light irradiation*

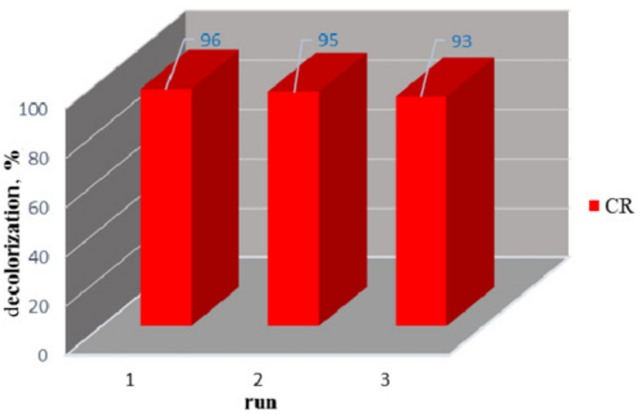

Fig. 11 *Recyclability of $ZnMn_2O_4$ NPs*

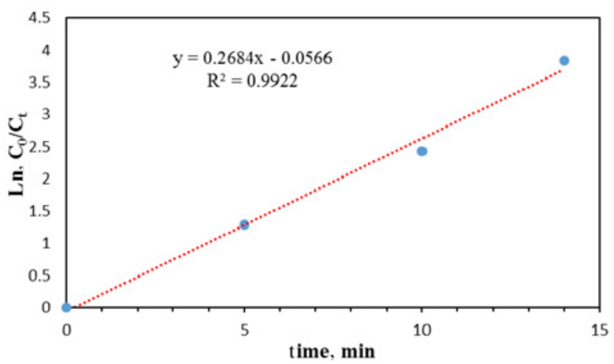

Fig. 12 *Plot of ln(C_0/C) versus time*

degradation efficiency decreased when the initial Congo red concentration enhanced. The considered proof is that by increasing the initial concentration of Congo Red, the photons get interrupted already can achieve the catalyst surface, therefore the absorption of photons decreases in the presence of a catalyst, and consequently, the degradation percent is reduced [38].

3.5. Effect of time on the degradation of Congo red: The UV–Vis spectra of the Congo red was considered for following degradation process in presence of $ZnMn_2O_4$ NPs as the photocatalyst at different time gap under the visible irradiation. Clearly, the maximum absorption peak of Congo red is found at 496 nm, with obvious diminution in intensity with raising irradiation time (Fig. 10). Approximately 96% of Congo red is degraded in 15 min. This evidence illustrates an important result that $ZnMn_2O_4$ NPs has a particular visible-light photocatalytic activity in degradation of the Cong red dye.

3.6. Reuse of the photocatalyst: The $ZnMn_2O_4$ NPs catalyst can be exerted frequently for the photocatalytic degradation of the dye solution. For measurement of the reusability of this catalyst, the photocatalytic degradation of Congo red under visible light irradiation was determined. This was done after gathering, washing with distilled water under ultrasonic irradiation and reusing the same photocatalyst for subsequent runs (Fig. 11). The photocatalyst did not exhibit any significant reduction in its activity even after three cycles. This is also confirmed that the $ZnMn_2O_4$ NPs was stable during the photocatalytic oxidation process. Moreover, these nanoparticles can be separated from the reaction solution using a centrifuge after degradation.

3.7. Kinetics of the photocatalytic degradation: The kinetics of the photocatalytic degradation of organic dyes generally follows the pseudo-first-order kinetics [39, 40]

$$\ln(C_0/C_t) = Kt$$

where k is the reaction rate constant. The photodegradation kinetics of Congo red parameters can be obtained by plotting the $\ln(C_0/C_t)$ versus time, the results are shown in Fig. 12. So, the values of correlation coefficient and rate constant for photocatalytic degradation of Congo red are determined to be 0.9922 and 0.2684 min^{-1}, respectively. Thus, the kinetics of degradation of Congo red is consistent with the pseudo-first-order kinetics model.

3.8. Comparison of dye photodegradation of $ZnMn_2O_4$ NPs with various catalysts: The degradation efficiency of the synthesised photocatalyst for Congo red dye degradation in comparison to those of other photocatalysts was shown in Table 1. It can be observed that some treatments caused a high value of degradation efficiency. While the reaction parameters containing catalyst dosage and irradiation time as compared to this work are higher.

Table 1 Photodegradation comparison of Congo red with diverse catalysts

Catalysts	Synthesis method	Dye	Dye concentration, mg/l	Catalyst dosage, mg	Light source	Irradiation time, min	Degradation activity, %	Refs.
CuO nanoleaves	low temperature aqueous growth	Congo red	20	50	UV-light	210	48	[41]
CuO nanorods	low temperature aqueous growth	Congo red	20	50	UV-light	210	67	[41]
CuO nanosheets	low temperature aqueous growth	Congo red	20	50	UV-light	210	12	[41]
ZnO NPs	co-precipitation	Congo red	20	50	solar radiation	120	85	[42]
ZnO NPs	sol–gel	Congo red	50	100	solar radiation	60	94	[43]
$ZnMn_2O_4$ NPs	sol–gel	Congo red	20	30	visible light	15	96	this study

doi: 10.1049/mnl.2019.0071

3.9. TOC removal: TOC removal of the Congo red solution has been considered under the optimised condition. Based on the results obtained from TOC and UV–Vis analysis, 96% of Congo red was degraded while only 45.2% of TOC of the Congo red solution was removed. Obviously, the TOC removal of the Congo red solution was less than the degradation of Congo red, proposing that the intermediates occurred during the photocatalytic reaction [44].

4. Conclusions: In the present work, we worked on a useful green method for synthesis of $ZnMn_2O_4$ NPs via sol–gel method using tragacanth gel. The results of the analysis confirm the synthesis of $ZnMn_2O_4$ in spinel structure with a single phase after calcination for 4 h at 600°C. In addition, the proposed method has significant advantages such as inexpensive, non-toxic, easy, environmentally friendly, non-toxic and free from any organic solvents and surfactant. The aqueous solution of Congo red is selected for considering the unique photocatalytic activity of $ZnMn_2O_4$ NPs. UV–Vis spectrophotometric studies confirm that 96% of Congo red dye is degraded after 15 min in natural pH, room temperature and under the visible light irradiation. Also, the synthesised photocatalyst provided TOC removal as 45.2% in 15 min. The kinetics of degradation of Congo red is consistent with the pseudo-first-order kinetics model. Obtained consequence states that this photocatalyst may be used to purify the water in various industries**.**

5 References

[1] Houas A., Lachheb H., Ksibi M., *et al.*: 'Photocatalytic degradation pathway of methylene blue in water', *Appl. Catal., B*, 2001, **31**, pp. 145–157

[2] Ullah H., Mushtaq L., Ullah Z., *et al.*: 'Cost effective green synthesis of NiO nanostructures as highly efficient photocatalysts for degradation of organic dyes', *Micro Nano Lett.*, 2019, **14**, pp. 103–106

[3] Patil S.S., Shinde V.M.: 'Biodegradation studies of aniline and nitrobenzene in aniline plant wastewater by gas chromatography', *Environ. Sci. Technol.*, 1988, **22**, pp. 1160–1165

[4] Kashefi S., Borghei S.M., Mahmoodi N.M.: 'Covalently immobilized laccase onto graphene oxide nanosheets: preparation, characterization, and biodegradation of azo dyes in colored wastewater', *J. Mol. Liq.*, 2019, **276**, pp. 153–162

[5] Kadirvelu K., Kavipriya M., Karthika C., *et al.*: 'Utilization of various agricultural wastes for activated carbon preparation and application for the removal of dyes and metal ions from aqueous solutions', *Bioresour. Technol.*, 2003, **87**, pp. 129–132

[6] Gao Y., Deng S.-Q., Jin X., *et al.*: 'The construction of amorphous metal-organic cage-based solid for rapid dye adsorption and time-dependent dye separation from water', *Chem. Eng. J.*, 2019, **357**, pp. 129–139

[7] Slokar Y.M., Majcen Le Marechal A.: 'Methods of decoloration of textile wastewaters', *Dyes Pigm.*, 1998, **37**, pp. 335–356

[8] Karunakaran C., JebaSingh I., Vinayagamoorthy P., *et al.*: 'Magnetically separable CdS-deposited Fe_3O_4-implanted ZnO microrods for solar photocatalysis', *IET Micro Nano Lett.*, 2014, **9**, pp. 529–531

[9] Liu Y., Jia X., Wu X.: 'Zno core-shell microspheres prepared by one-pot hydrothermal reaction and their photocatalysis properties', *IET Micro Nano Lett.*, 2014, **9**, pp. 328–331

[10] Battiston S., Rigo C., Severo E.d.C., *et al.*: 'Synthesis of zinc aluminate ($ZnAl_2O_4$) spinel and its application as photocatalyst', *Mater. Res.*, 2014, **17**, pp. 734–738

[11] Menaka J., Qamar M., Lofland S.E., *et al.*: 'Magnetic and photocatalytic properties of nanocrystalline ZnMn2O4', *Bull. Mater. Sci.*, 2009, **32**, pp. 231–237

[12] Ahmadi F., Rahimi-Nasrabadi M., Behpour M.: 'Synthesis Nd_2TiO_5 nanoparticles with different morphologies by novel approach and its photocatalyst application', *J. Mater. Sci. Mater. Electron.*, 2017, **28**, pp. 1531–1536

[13] Ramezani M., Hosseinpour-Mashkani S.M., Sobhani-Nasab A., *et al.*: 'Synthesis, characterization, and morphological control of $ZnMoO_4$ nanostructures through precipitation method and its photocatalyst application', *J. Mater. Sci. Mater. Electron.*, 2015, **26**, pp. 7588–7594

[14] Atrak K., Ramazani A., Taghavi Fardood S.: 'A novel sol–gel synthesis and characterization of $MgFe_2O_4$@γ–Al_2O_3 magnetic nanoparticles using tragacanth gel and its application as a magnetically separable photocatalyst for degradation of organic dyes under visible light', *J. Mater. Sci. Mater. Electron.*, 2018, **29**, pp. 6702–6710

[15] Moradi S., Taghavi Fardood S., Ramazani A.: 'Green synthesis and characterization of magnetic $NiFe_2O_4$@ZnO nanocomposite and its application for photocatalytic degradation of organic dyes', *J. Mater. Sci. Mater. Electron.*, 2018, **29**, pp. 14151–14160

[16] Shojaei A.F., Tabari A.R., Loghmani M.H.: 'Normal spinel $CoCr_2O_4$ and $CoCr_2O_4/TiO_2$ nanocomposite as novel photocatalysts, for degradation of dyes', *IET Micro Nano Lett.*, 2013, **8**, pp. 426–431

[17] Atrak K., Ramazani A., Taghavi Fardood S.: 'Green synthesis of amorphous and gamma aluminum oxide nanoparticles by tragacanth gel and comparison of their photocatalytic activity for the degradation of organic dyes', *J. Mater. Sci. Mater. Electron.*, 2018, **29**, pp. 8347–8353

[18] Bangale S.V., Bamane S.R.: 'Preparation and electrical properties of nanostructured spinel $ZnCr_2O_4$ by combustion route', *J. Mater. Sci. Mater. Electron.*, 2013, **24**, pp. 277–281

[19] Sorbiun M., Shayegan Mehr E., Ramazani A., *et al.*: 'Green synthesis of zinc oxide and copper oxide nanoparticles using aqueous extract of oak fruit hull (jaft) and comparing their photocatalytic degradation of basic violet 3', *Int. J. Environ. Res.*, 2018, **12**, pp. 29–37

[20] Alagiri M., Hamid S.B.A.: 'Green synthesis of α-Fe_2O_3 nanoparticles for photocatalytic application', *J. Mater. Sci. Mater. Electron.*, 2014, **25**, pp. 3572–3577

[21] Hosseini S.A., Moalemzade P.: '$Cufe_{2-x}Lu_xO_4$ nanoparticles: synthesis through a green approach and its photocatalyst application', *J. Mater. Sci. Mater. Electron.*, 2016, **27**, pp. 8802–8806

[22] Saeidian H., Moradnia F.: 'Benign synthesis of N-aryl-3,10-dihydroacridin-1(2H)-one derivatives via ZnO nanoparticle-catalyzed Knoevenagel condensation/intramolecular enamination reaction', *Iran. Chem. Commun.*, 2017, **5**, pp. 252–261

[23] Taghavi Fardood S., Ramazani A.: 'Black tea extract mediated green synthesis of copper oxide nanoparticles', *J. Appl. Chem. Res.*, 2018, **12**, pp. 8–15

[24] Meshram S.M., Bonde S.R., Gupta I.R., *et al.*: 'Green synthesis of silver nanoparticles using white sugar', *IET Nanobiotechnol.*, 2013, **7**, pp. 28–32

[25] Hoseinpour V., Souri M., Ghaemi N.: 'Green synthesis, characterisation, and photocatalytic activity of manganese dioxide nanoparticles', *Micro Nano Lett.*, 2018, **13**, pp. 1560–1563

[26] Taghavi Fardood S., Ramazani A., Golfar Z., *et al.*: 'Green synthesis using tragacanth gum and characterization of Ni–Cu–Zn ferrite nanoparticles as a magnetically separable catalyst for the synthesis of hexabenzylhexaazaisowurtzitane under ultrasonic irradiation', *J. Struct. Chem.*, 2018, **59**, pp. 1730–1736

[27] Taghavi Fardood S., Ramazani A., Moradi S., *et al.*: 'Green synthesis of zinc oxide nanoparticles using arabic gum and photocatalytic degradation of direct blue 129 dye under visible light', *J. Mater. Sci. Mater. Electron.*, 2017, **28**, pp. 13596–13601

[28] Shabanalizadeh S., Abedini A., Alborzi A., *et al.*: 'Green synthesis and characterization of lead titanate nanoparticles and its photocatalyst application', *J. Mater. Sci. Mater. Electron.*, 2016, **27**, pp. 2589–2593

[29] Shayegan Mehr E., Sorbiun M., Ramazani A., *et al.*: 'Plant-mediated synthesis of zinc oxide and copper oxide nanoparticles by using ferulago angulata (schlecht) boiss extract and comparison of their photocatalytic degradation of rhodamine B (RhB) under visible light irradiation', *J. Mater. Sci. Mater. Electron.*, 2018, **29**, pp. 1333–1340

[30] Zhang N., Fu X., Xu Y.-J.: 'A facile and green approach to synthesize Pt@CeO_2 nanocomposite with tunable core-shell and yolk-shell structure and its application as a visible light photocatalyst', *J. Mater. Chem.*, 2011, **21**, pp. 8152–8158

[31] Yoon T.P., Ischay M.A., Du J.: 'Visible light photocatalysis as a greener approach to photochemical synthesis', *Nat. Chem.*, 2010, **2**, p. 527

[32] Taghavi Fardood S., Ramazani A., Joo S.W.: 'Eco-friendly synthesis of magnesium oxide nanoparticles using arabic Gum', *J. Appl. Chem. Res.*, 2018, **12**, pp. 8–15

[33] Taghavi Fardood S., Golfar Z., Ramazani A.: 'Novel sol–gel synthesis and characterization of superparamagnetic magnesium ferrite nanoparticles using tragacanth gum as a magnetically separable

doi: 10.1049/mnl.2019.0071

photocatalyst for degradation of reactive blue 21 dye and kinetic study', *J. Mater. Sci. Mater. Electron.*, 2017, **28**, pp. 17002–17008
[34] Thangaraj V., Mahmud S., Li W., ET AL.: 'Greenly synthesised silver-alginate nanocomposites for degrading dyes and bacteria', *IET Nanobiotechnol.*, 2017, **12**, pp. 47–51
[35] Gholipour N., Rahimi-Nasrabadi M.: 'Auto-combustion preparation and characterization of $BaFe_2O_4$ nanostructures by using lemon juice as fuel', *Chem. Method.*, 2019, **3**, pp. 276–282
[36] Zhang P., Li X., Zhao Q., ET AL.: 'Synthesis and optical property of one-dimensional spinel $ZnMn_2O_4$ nanorods', *Nanoscale Res. Lett.*, 2011, **6**, p. 323
[37] Nouri J., Khoshravesh T., Khanahmadzadeh S., ET AL.: 'Synthesis, characterization and optical band gap of lithium cathode materials: $Li_2Ni_8O_{10}$ and $LiMn_2O_4$ nanoparticles', *Int. J. Nano Dimens.*, 2016, **7**, pp. 15–24
[38] Reza K.M., Kurny A., Gulshan F.: 'Parameters affecting the photocatalytic degradation of dyes using TiO_2: a review', *Appl. Water Sci.*, 2017, **7**, pp. 1569–1578
[39] Bai L., Zheng S., Li Z., ET AL.: 'Design of Ag-decorated ZnO concave nanocubes using ZIF-8 with dual functional catalytic ability for decoloring dyes', *CrystEngComm*, 2018, **20**, pp. 2980–2988
[40] Zheng Y., Zheng L., Zhan Y., ET AL.: 'Ag/ZnO heterostructure nanocrystals: synthesis, characterization, and photocatalysis', *Inorg. Chem.*, 2007, **46**, pp. 6980–6986
[41] Sadollahkhani A., Ibupoto Z.H., Elhag S., ET AL.: 'Photocatalytic properties of different morphologies of CuO for the degradation of Congo red organic dye', *Ceram. Int.*, 2014, **40**, pp. 11311–11317
[42] Adam R.E., Pozina G., Willander M., ET AL.: 'Synthesis of ZnO nanoparticles by co-precipitation method for solar driven photodegradation of Congo red dye at different pH', *Photonics Nanostruct. Fundam. Appl.*, 2018, **32**, pp. 11–18
[43] Ong C.B., Mohammad A.W., Rohani R., ET AL.: 'Solar photocatalytic degradation of hazardous Congo red using low-temperature synthesis of zinc oxide nanoparticles', *Process Saf. Environ. Prot.*, 2016, **104**, pp. 549–557
[44] Khadhraoui M., Trabelsi H., Ksibi M., ET AL.: 'Discoloration and detoxicification of a Congo red dye solution by means of ozone treatment for a possible water reuse', *J. Hazard. Mater.*, 2009, **161**, pp. 974–981